PAPER

Gold nanoclusters based dual-emission hollow TiO$_2$ microsphere for ratiometric optical thermometry†

Chuanxi Wang,*[a] Yijun Huang,[a] Huihui Lin,[a] Zhenzhu Xu,[a] Jiapeng Wu,[a] Mark G. Humphrey[b] and Chi Zhang*[a]

In this work, we develop a novel dual-emitting hollow TiO$_2$ microsphere with high stability and attractive thermal sensitivity, which could work as nanosensor for accurately measuring temperature. This nanosensor is prepared through coating gold nanocluster (AuNCs) on the surface of carbon dots-doped hollow TiO$_2$ microsphere. As-prepared nanosensor shows characteristic dual-emitting property of carbon dots (CDs, blue fluorescence) and AuNCs (red fluorescence) under a single excitation wavelength. Moreover, upon increasing the temperature, the intensity of red emission from the AuNCs continuously quenched, whereas that of blue emission from the CDs remained nearly constant. The different response results in a continuous fluorescence color change from red to purple that can be clearly observed by the naked eyes. Thus, as-prepared dual-emitting hollow TiO$_2$ microsphere could be used as optical thermometry by taking the advantage of the temperature sensitivity of their fluorescence intensity ratio (red/blue) with high reliability and accuracy, which change considerably over the wide temperature range (20–80 °C) with small temperature resolution (~0.5 °C). Additionally, this nanosensor is successfully applied in 10 mM buffered saline (PBS) solution with physiological temperature ranging from 20 to 45 °C, which suggests as-prepared dual-emitting microspheres have promising applications *in vivo* temperature sensing.

1. Introduction

Metal nanoclusters (NCs) with discrete energy levels possess molecule-like electronic transitions within their conduction bands, and may exhibit unique physical and chemical properties including strong luminescence, as well as have potential practical applications in, for example, cell labelling, ion sensing, and catalysis.[1–4] Similar to quantum dots, these small clusters exhibit tunable fluorescence from visible to near-infrared regions due to molecule-like electronic transitions within the conduction bands or the charge-transfer transition from the ligand to metal nanoparticles.[5–7] In addition, these clusters exhibit high photoluminescence (PL) quantum yield, and could be handily synthesized.[8,9] Among them, luminescent gold NCs (AuNCs) are attractive for a wide variety of biomedical applications, such as biosensing, *in vitro* and *in vivo* imaging, and also in cancer therapy, owing to their low toxicity, good biocompatibility and multifunctional surface chemistry.[10,11] More importantly, AuNCs showed temperature sensitivity of their luminescence and could be used recently as versatile nanothermometry devices in living cells.[12,13] However, this kind of intensity-based temperature sensors would be affected by local environment including oxygen content, pH, concentration and usually gave inaccurate temperature information.[14] It is well known that temperature is one of the most important parameters that governs biological reactions within a living cell.[15,16] The accurate measurement of temperature and its gradient inside a live cell can promote the advancements in cell biology and biomedicine, for example, the cellular pathogenesis of cancer is characterized by extraordinary heat production.[17]

Recently, dual-emitting temperature sensors have attracted much attention since they operate as "non-contact" tools and accurately measure temperature.[18–20] With such a sensor, a change in temperature leads to a measurable change in the relative rather than absolute PL intensities of one or both the states.[21] This reduces the impact of extrinsic factors like fluctuations in excitation rate, detection efficiency, probe concentration, optical occlusion, or other local inhomogeneity. To date, several dual-emitting nanomaterials, such as CdSe/ZnS nanocrystals, rare earth-doped nanoparticles and polymer dots have already shown a great potential for nanothermometry in biological systems, and especially live cells.[22–25] For example,

[a]*China-Australia Joint Research Centre for Functional Molecular Materials, School of Chemical & Material Engineering, Jiangnan University, Wuxi 214122, P. R. China. E-mail: wangcx@jiangnan.edu.cn; chizhang@jiangnan.edu.cn*

[b]*Research School of Chemistry, Australian National University, Canberra, ACT 0200, Australia*

† Electronic supplementary information (ESI) available. See DOI: 10.1039/c5ra13475g

CdSe/ZnS core–shell quantum dots have been demonstrated temperature-sensitive fluorescence, which is used as thermal nanoprobe for temperature sensing in liquids and HeLa cervical cancer cells.[24] Unfortunately, the high toxicity or instability limited their further application. Therefore, it is practical to develop a novel dual-color fluorescence sensor based on ratiometric signal output for rapid visual identification of temperature. On the other hand, carbon dots (CDs) and NCs, as two important class of PL nanomaterials, have been applied widely in the fields of bioimaging, printing inks, photocatalysis, and sensors.[26–28] CDs or NCs based dual-emitting nanomaterials could work as nanosensors for Cu^{2+}, Hg^{2+} and highly reactive oxygen species,[29–31] while no literature has reported CDs(NCs)-based dual-emitting probes for ratiometric temperature detection.

Herein, the novel dual-emitting microspheres are designed using the blue fluorescent CDs and red fluorescent AuNCs as fluorophores. Resultant microspheres showed dual-emitting fluorescence in blue and red region. The red fluorescence came from the AuNCs on the surface of microspheres which showed temperature responsive optical properties; in contrary, the blue fluorescence of CDs in the core of microspheres would not change. Hence, such dual-emitting microspheres could be used as nanosensors for accurate measurement of temperature. Moreover, owing to TiO_2 layer as scaffolds, resultant dual-emitting temperature sensors showed good biocompatibility and high stability. These features suggested resultant dual-emitting nanosensors could be promising nanothermometry in living cells.

2.   Experimental

2.1   Materials

Reduced glutathione (GSH, molecular weight of 307 g mol^{-1}), 1-octadecene (ODE, 90%), oleic acid (OA, 90%), oleyl amine (OLA, 70%), (3-aminopropyl)trimethoxysilane (APS), 1-ethyl-3-(3-dimethylaminopropyl)carboxylate (EDC) and N-hydroxysuccinimide (NHS) were purchased from Aldrich. Tetrachloroauric(III) acid (HAuCl$_4$), citric acid monohydrate (CA), titanium butoxide (TBOT, 98%), ethylene glycol, acetone, Tween 20, chloroform, and methanol were purchased from Sinopharm Chemical Reagent Co., Ltd (China). All reagents were used as received without further purification. The solutions of 200 mM NaCl, KNO$_3$, Ca(NO$_3$)$_2$, MgSO$_4$ were prepared, respectively. Deionized water was used in all experiments.

2.2   Preparation of fluorescent carbon dots and gold nanoclusters

According to the previously reported method, gold nanoclusters (AuNCs) were synthesized by a green thermal reduction approach with GSH as both reducing and stabilizing agents.[32,33] Briefly, 20×10^{-3} M HAuCl$_4$ (0.5 mL) was added to deionized water (15 mL) followed by the adding 5 mL GSH (0.0150 g) solution. The mixture was stirred at 25 °C for 5 min, and then continuously stirred for 8 h at 100 °C. The purification of resultant GSH-AuNCs was centrifuging at 12 000 rpm to remove

large particles. Resultant AuNCs were stored at 4 °C for further using.

The carbon dots (CDs) were prepared by a similar organic-based surface-capping method.[34] In typical process, the mixture of CA (0.42 g, 2 mmol), OA (3 mL, 8.7 mmol), OLA (0.3 mL, 0.62 mmol), and ODE (7 mL, 19.8 mmol) were degassed at room temperature and heated up to 100 °C under vacuum for 1 h with stirring. The resultant homogeneous solution was switched to a dry nitrogen atmosphere, heated to 250 °C slowly and maintained at this temperature for 1 h. The color of the solution became transparent with raising temperature and finally turned to dark brown. The temperature of the solution was dropped under 100 °C. The resultant CDs were precipitated by addition of methanol, rinsed with methanol, and then re-dispersed in 10 mL of chloroform for further using.

2.3   Preparation of dual-emitting microspheres

The blue PL CDs-doped TiO_2 microspheres would be prepared by sol–gel method.[35] 0.05 mL of TBOT was added to 10 mL ethylene glycol under stirring for 8 h at room temperature, then 3 mL of the mixture of TBOT and ethylene glycol was added into the 40 mL acetone containing 0.2 mL Tween 20 and 2 mL CDs. After agitation for 24 h, the resultant microspheres were collected by centrifugation and washed three times with ethanol, and then re-dispersed in 5 mL of ethanol for further using.

To prepare the dual-emitting microspheres, we firstly modified the TiO_2 microspheres with APS as follows: the CDs-doped TiO_2 microspheres (5 mL) were mixed with APS (10 μL), and stirred for 12 h. The resultant products were centrifuged and washed with ethanol and water several times, and then re-dispersed in 5 mL water solution. The dual-emitting microspheres were built through carbodiimide-activated coupling reaction between GSH-AuNCs and amino-functionalized TiO_2 microspheres. Typically, 25 mg EDC and 15 mg of NHS were added to 3 mL of PBS buffer (pH = 6.86) containing 10 mg GSH-AuNCs, and then mixed with 2 mL of aqueous solution containing 20 mg of amino-functionalized TiO_2 microspheres. This solution was allowed to react under magnetic stirring for 24 h. Finally, the resultant dual-emitting microspheres were collected through centrifugation at 6000 rpm and washed three times with water, and then re-dispersed in 5 mL aqueous solution for further application.

2.4   Temperature-dependent fluorescence of dual-emitting microspheres

To test the temperature dependence of fluorescence, temperature was controlled in the range from 20 to 80 °C and the fluorescence intensity of dual-emitting microspheres towards different temperature values were monitored with a spectrofluorimeter.

2.5   Calibration curve and temperature resolution of the dual-emission fluorescent nanosensor

The calibration curve for temperature with dual-emitting microspheres was obtained by approximating the relationship

between averaged ratio of fluorescence intensity at 596 nm and 436 nm ($n = 3$) and temperature to the third-order polynomial (with OriginPro-2012, $r^2 = 0.99$, 20 °C < T < 80 °C)

$$R(T) = 7.21699 \times 10^{-8}T^3 + 7.06814 \times 10^{-7}T^2 - 0.00896 \times T + 1.15089 \quad (1)$$

where T and $R(T)$ represent temperature and ratio of fluorescence intensity at 596 nm and 436 nm at T °C, respectively.

The temperature resolution (δT) of dual-emitting microspheres was evaluated using the following equation:

$$\delta T = \left(\frac{\partial T}{\partial R}\right)\delta R \quad (2)$$

where $\partial T/\partial R$ and δR represent the inverse of the slope of the fluorescence ratio–temperature diagram and the SD of the fluorescence ratio, respectively. The SD value was obtained by triplicate measurements of one sample at each temperature.

2.6 Characterization methods

Photoluminescence (PL) experiments were performed with a Cary Eclipse spectrofluorimeter (Varian, America). X-ray photoelectron spectroscopy (XPS) using Mg K_α excitation (1253.6 eV) was collected in a VG ESCALAB MKII spectrometer. Binding energy calibration was based on C 1s at 284.6 eV. The morphology and mean diameter of the resultant samples were characterized by scanning electron microscopy (SEM, Hitachi S4800) and transmission electron microscopy (TEM, JEM-2100).

3. Results and discussion

3.1 Synthesis and characterization of dual-emitting microspheres

The fabrication process of the dual-emitting hollow microspheres were shown in Fig. 1. In the first step, the carbon dots (CDs) were prepared by organic-based surface-capping method.[34] The citric acid (CA) worked as C source which would carbonized under high temperature to form CDs and gave off strongly blue photoluminescence (PL). Moreover, as-prepared CDs exhibited good dispersion and high stability in chloroform solution due to the OA and OLA as surface passivation. Using typical sol–gel method,[35] the hollow CDs/TiO$_2$ microspheres were prepared and as-prepared microspheres displayed the blue PL of CDs. Moreover, the TiO$_2$ surface can be modified with suitable functional groups, such as thiol, carboxyl, and amine groups.[36–38] Herein, the surface of CDs/TiO$_2$ hollow microspheres would be modified with amine groups through conjugating with (3-aminopropyl)trimethoxysilane (APS). Then the dual-emission fluorescent hollow microspheres could be formed through carbodiimide-activated coupling reaction between glutathione stabilized gold nanoclusters (GSH-AuNCs, red PL) and amino-functionalized CDs/TiO$_2$ hollow microspheres (blue PL).[39]

The optical properties of resultant products were displayed in Fig. 2. In chloroform solution, resultant CDs showed an emission peak at 436 nm upon excitation at 365 nm (Fig. 2a). Moreover, the diluted solution of the as-prepared CDs in
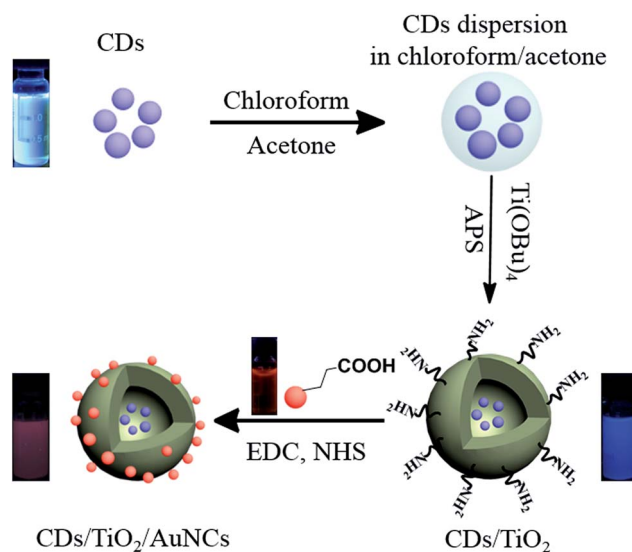

Fig. 1 Schematic illustration of the preparation of ratiometric dual-emission fluorescent hollow microspheres.

chloroform solution was slight yellow color under visible light (Fig. S1a†), while it emitted blue fluorescence under UV light illumination ($\lambda_{ex} = 365$ nm) (inset of Fig. 1). After forming the CDs/TiO$_2$ hollow microspheres, the blue fluorescence of CDs was observed, thus as-prepared microspheres exhibited intense blue emission under 365 nm UV light (inset of Fig. 1) and good dispersion in aqueous solution (Fig. S1b†). The AuNCs were prepared by a green thermal reduction approach without any noxious reducing agent, such as NaBH$_4$ or N$_2$H$_4$·2H$_2$O.[40,41] GSH, a naturally occurring and readily available tripeptide, functions as both reducing agent and stabilizing agent in the thermal reduction process.[32,33] As-prepared AuNCs showed good dispersion in aqueous solution and red PL with an emission peak at 596 nm (Fig. 2c), and a highly red fluorescence can be clearly observed under a UV lamp ($\lambda_{ex} = 365$ nm) (inset of Fig. 1).

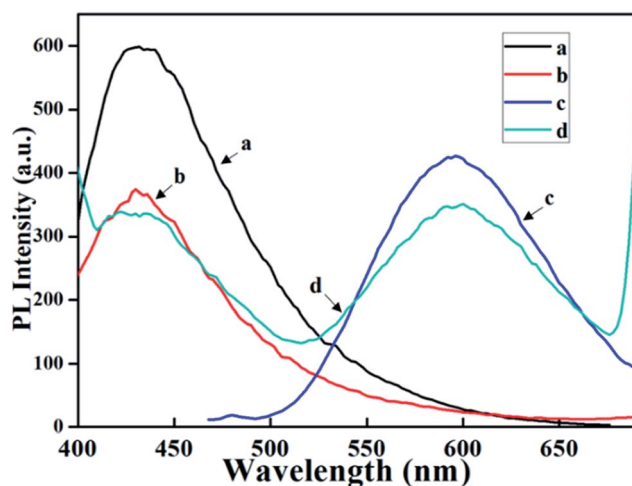Fig. 2 Fluorescence spectra of (a) CDs; (b) CDs/TiO$_2$ hollow microspheres; (c) AuNCs; (d) dual-emission fluorescent hollow microspheres.

Moreover, as a natural biomolecule, GSH owned several functional groups including carboxyl and amino groups, made NCs be beneficial for their surface modification to achieve further applications in wide range.[11,42] Herein, dual-emission fluorescent nanosensor can be formed by carbodiimide-activated coupling of GSH-AuNCs (red PL) and amino-functionalized CDs/TiO$_2$ hollow microspheres (blue PL). Following excitation at a single wavelength (365 nm), the hollow microspheres exhibited two different luminescence peaks, one from the AuNCs (red PL) and the other from the CDs (blue PL), as shown in Fig. 2d.

Then the morphology and structure of resultant products were confirmed by transmission electron microscope (TEM) and X-ray photoelectron spectroscopy (XPS). As shown in Fig. 3a, as-prepared CDs were distributed in the range from 1.8 to 3.6 nm with an average size of 2.5 nm. Moreover, there were no formation of larger size C nanoparticles or aggregation due to OA and OLA as surface passivation agent.[34] And TEM image indicated that the as-prepared AuNCs had a uniform dispersion without apparent aggregation and particle diameters were 1.6–2.5 nm with the average size of 2.1 nm (Fig. 3c). The size distribution of CDs and AuNCs were shown in Fig. S2.† It is well known that the organic-soluble CDs could be easily wrapped by the TiO$_2$ shell to avoid the direct contact of CDs with components in the sample. In this procedure, CDs were extremely stable in chloroform solution as a nonpolar solvent. However, organic-soluble were unstable in acetone/chloroform mixture since acetone is a polar solvent and particles incline to self-assemble into clusters in the mixture of solvents.[43,44] This may cause the fact that emulsion drops would be formed by the acetone as the emulsifier when chloroform-suspended nanoparticles were added to acetone.[45] During the sol–gel process, the hollow structure usually appeared.[46,47] The morphology of CDs/TiO$_2$ microspheres was confirmed by TEM and SEM. As shown in Fig. 3b, the as-prepared CDs/TiO$_2$ hollow microspheres were fairly uniform in shape and size, and the average diameter of the microspheres was about 207 nm with shell

thicknesses of 66 nm. Seeing the SEM image (Fig. S3†), we known that the surfaces of the resultant CDs/TiO$_2$ microspheres were very smooth.

To build the dual-emitting ratiometric nanosensor, the GSH-AuNCs are conjugated with formed CDs/TiO$_2$ hollow microspheres. Their architecture of the ratiometric nanosensors are studied in detail. TEM image indicated that the as-prepared ratiometric nanosensors were well-dispersed with the average size of about 210 nm and the shell thicknesses were 58 nm (Fig. 3d). As can be seen, the surface of CDs/TiO$_2$ hollow microsphere was very smooth (Fig. 3b). Different from them, as-prepared dual-emitting ratiometric nanosensor showed a comparatively rough surface (Fig. 3d), suggesting the successful attachment of AuNCs on the surfaces of CDs/TiO$_2$ hollow microspheres. Although the size of TiO$_2$ microspheres was larger than 200 nm, there was no PL signal in their solution with various concentrations (Fig. S4a†). While the PL of dual-emission microspheres decreased with decreasing the concentration, but the PL intensity ratio would not change with various concentrations (Fig. S4b†), which confirmed the blue PL came from the doped CDs, rather than the scattering of TiO$_2$ microspheres. When the GSH-AuNCs were coated on the surface of the CDs/TiO$_2$ hollow microspheres, a well-resolved dual emission spectrum peaked at 436 nm and 596 nm was displayed at a single excitation wavelength (365 nm) (Fig. 2d). The corresponding fluorescence color of the ratiometric nanosensor was shown in Fig. 2d for a direct comparison with those of the blue emission CDs/TiO$_2$ (Fig. 2b) and the red emission AuNCs (Fig. 2c). Clearly, a significant change of fluorescence color under a UV ($\lambda = 365$ nm) lamp was observed (inset of Fig. 1). Moreover, the elemental composition of dual-emission fluorescent microspheres were confirmed by XPS. The binding energy of Au 4f located at 88.1 eV and 84.3 eV respectively (Fig. S5a†) could explicitly demonstrate that the electronic structure of AuNCs.[48] The binding energy of C 1s was matched with the previously prepared CDs (Fig. S5b†).[34,49] Thus, these results indicated that the red emission AuNCs were successfully conjugated onto the surface of the blue CDs-embedded TiO$_2$ hollow microspheres and resultant products showed dual-emitting PL under a single excitation.
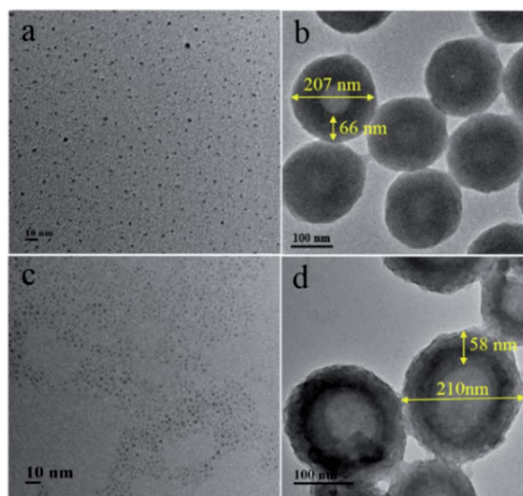
3.2 High stability of dual-emitting nanosensor

The stability of luminescent nanomaterials is an important factor to assess their applications.[11,50] Therefore, to demonstrate effective detection performances of dual-emitting nanosensor, the stability of the nanosensor was firstly investigated. As shown in Fig. 4a, the photo-stability of the as-prepared ratiometric nanosensor was systematically investigated by exposing them under a 450 W xenon (Xe) lamp for various time spans. The relative corresponding effect can be quantitatively evaluated by analyzing the dependence of the PL intensity ratio (I_{596}/I_{436}). After 12 consecutive illumination at 365 nm (10 min for each time), the relative fluorescence intensity ratio had no apparent change, implying the photo-stability of the ratiometric fluorescence nanosensor in aqueous solution (Fig. 4a). The fluorescence spectra of the ratiometric fluorescence nanosensor

Fig. 3 TEM image of (a) CDs; (b) CDs/TiO$_2$ hollow microspheres; (c) AuNCs; (d) dual-emission fluorescent microspheres.
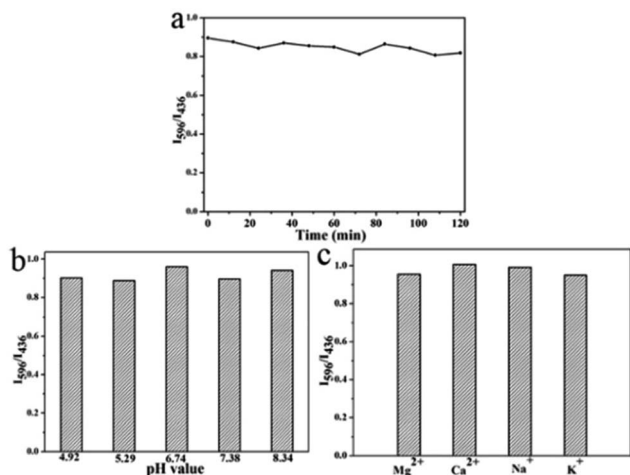
Fig. 4 The fluorescent stability of dual-emission nanosensor: (a) photo-stability of as-prepared nanosensor radiated by a 450 W Xe light at various time; (b) the pH stability of nanosensor in pH range from 4.9 to 8.3; (c) the metal stability of nanosensor in various metal ions with the concentration of 200 mM.
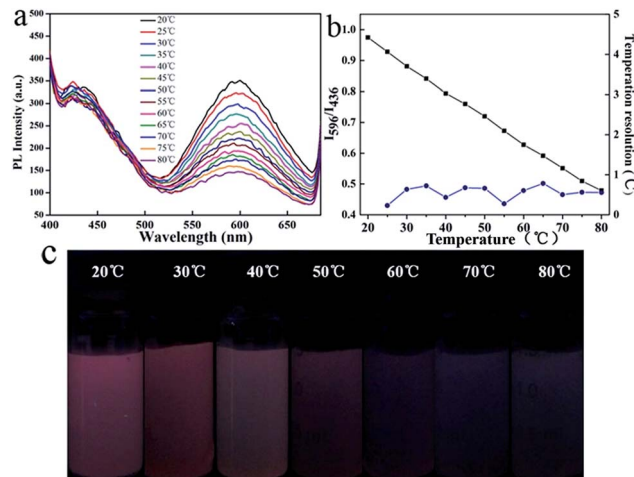

Fig. 5 (a) PL spectra of dual-emission fluorescent nanosensor with increasing temperature from 20 to 80 °C (top to bottom); (b) the ratio of the intensity at 596 nm and 436 nm (I_{596}/I_{436}) is plotted versus temperature and good temperature resolution (blue line, right axis); (c) fluorescence photographs of the ratiometric nanosensor are taken under a UV lamp with an excitation wavelength at 365 nm.

irradiated by a Xe lamp at various time in detail were shown in Fig. S6a.†

When the fluorescence nanosensors are used for intracellular nanothermometry, the materials must keep stable toward intracellular environments. PL intensity ratio of the fluorescence nanosensors toward physiological pH and physiological ions in solution were measured. Fig. 4b presented the PL intensities of fluorescent nanosensor at different pH values. The results revealed that the material displayed stable fluorescence intensity ratio with different pH values. We also investigated the effect of ionic strength on the stability of fluorescent nanosensor in the solution containing different ions. As shown in Fig. 4c, even in the physiological ionic strength (200 mM of KCl or NaCl), the PL intensity-ratio remained constant with different ions. The fluorescence spectra of the ratiometric fluorescence nanosensor toward physiological pH and physiological ions in detail in Fig. S6b and c.† Compared to previously reported dual-emitting nanosensors,[18,25] as-prepared dual-emitting hollow microspheres indicated ultra-stable PL in solution environment due to the TiO$_2$ as a protective shell. Moreover, this novel dual-emitting hollow microspheres could be easy purification. Therefore, these advantages made them have particular appropriate for practical applications.

3.3 Optical response of dual-emitting nanosensor toward temperature

To explore the potential applications of the dual-emitting hollow microspheres as ratiometric optical thermometry, we investigated their temperature-dependent response. The fluorescence responses toward temperature of them were measured at the temperature ranged from 20 to 80 °C (Fig. 5a). According to previous research, GSH-AuNCs could work as versatile nanothermometry devices by taking advantage of the temperature sensitivity of their fluorescence lifetime and emission intensity.[13] Therefore, upon increasing the temperature, the
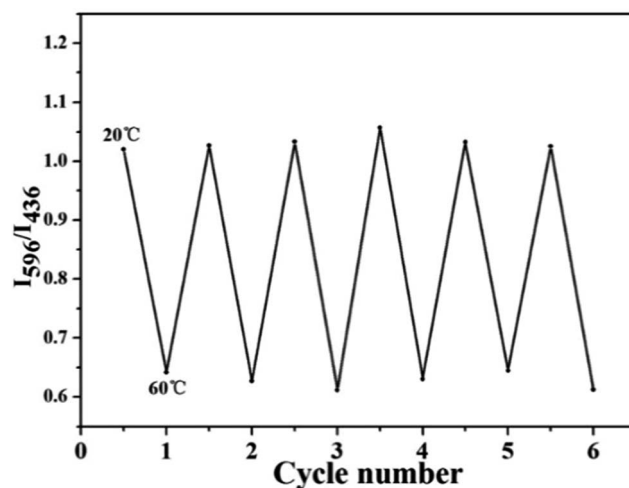

Fig. 6 Temperature-induced switching of the emission intensities ratio of the dual-emitting nanosensor (alternating between 20 °C and 60 °C).

intensity of red emission from the reactive GSH-AuNCs showed continuous quenching, whereas that of blue emission from the CDs still remained constant (Fig. 5a). As shown in Fig. 5b, there is a good linear relationship between temperature and fluorescence intensity ratio. This linear relationship can be fitted as a function of $R(T) = 1.13286 - 8.3 \times 10^{-3}T$ with correlation coefficient 0.998, where T and $R(T)$ represent temperature and ratio of fluorescence intensity at 596 nm and 436 nm. Moreover, the temperature resolution, evaluated as the product of the inverse of the slope of intensity ratio versus temperature and the standard deviation of the averaged fluorescent intensity ratio, was determined to be smaller than 0.5 °C (Fig. 5b), which is better than the resolution of previous fluorescent thermometers.[24,25,51] Thus the fluorescent nanosensor could be acted as an

ideal ratiometric temperature sensor with high reliability and accuracy. Clearly, a distinguishable color change from original red to purple that can be clearly observed by the naked eyes (Fig. 5c). To further investigate the reproducibility of fluorescent nanosensor, the luminescence switching operations were repeated for six consecutive cycles by multiple heating and cooling cycles between 20 and 60 °C. The results are presented in Fig. 6, and the corresponding spectra are shown in Fig. S7.† This fatigue-resistant performance suggests that the dual-emitting hollow microspheres may be applicable as PL thermometers and biosensors in cell monitoring.

This dual-emission fluorescent temperature sensor could be useful in the 10 mM phosphate buffered saline (PBS) solution (pH = 7.4, Fig. S8†) and the ratios of fluorescence intensities showed a linear relationship with increasing temperature from 20 to 45 °C. Given this temperature range is larger than the physiological temperature, which suggests the as-prepared fluorescent nanosensor has promising applications *in vivo* temperature sensing. Compared with traditional intensity-based temperature sensors,[52,53] this novel dual-emitting sensors show resolvable luminescence emissions from two different excited states. When temperature changed one or both of these PL intensities, its effect is measurable from relative instead of absolute PL intensities, reducing the impact of extrinsic factors like fluctuations in excitation rate, detection efficiency, probe concentration, optical occlusion, or other local inhomogeneities that alter absolute PL intensities.[21] Although the size of as-prepared dual-emitting microsphere is large, similar microspheres have been applied in cellular imaging.[29,32,39,54] Moreover, this dual-emitting microspheres show dual-emitting property under a single excitation wavelength, small temperature resolution (0.5 °C), high stability and good dispersion in aqueous solution. Additionally, as-prepared dual-emitting microspheres could be used as optical thermometry over the wide temperature range (20–80 °C) aqueous solution and in PBS solution with physiological temperature ranging from 20 to 45 °C, which suggests they have promising applications *in vivo* temperature sensing.

4. Conclusion

In summary, the novel dual-emitting microspheres were synthesized using the blue fluorescent CDs and red fluorescent AuNCs as fluorophores. Resultant microspheres showed an ideal single-excitation, dual emission fluorescence with peaks at 436 nm (blue PL) and 596 nm (red PL), respectively. The red fluorescence came from the AuNCs on the surface of microspheres which showed temperature responsive optical properties; in contrary, the blue fluorescence of CDs in the core of microspheres would not change towards temperature. The intensity ratio of the two emission wavelengths (I_{596}/I_{436}) showed a linear relationship with increasing temperature from 20 to 80 °C. Hence, such dual-emitting nanocomposites could be used as nanosensors for accurate measurement of temperature. Moreover, owing to TiO$_2$ layer as scaffolds, resultant dual-emitting temperature sensors showed good biocompatibility and high stability. These features suggested resultant dual-emitting nanosensors could be promising in offering the dual function of cellular imaging and temperature sensing at the molecular level.

Notes and references

1 Y. Z. Lu and W. Chen, *Chem. Soc. Rev.*, 2012, **41**, 3594–3623.
2 G. Li and R. C. Jin, *Acc. Chem. Res.*, 2013, **46**, 1749–1758.
3 Y. Chen, H. P. Zhou, Y. Wang, W. Y. Li, J. Chen, Q. Lin and C. Yu, *Chem. Commun.*, 2013, **49**, 9821–9823.
4 C. Wang, C. X. Wang, L. Xu, H. Cheng, Q. Lin and C. Zhang, *Nanoscale*, 2014, **6**, 1775–1781.
5 S. Choi, R. M. Dicksonc and J. Yu, *Chem. Soc. Rev.*, 2012, **41**, 1867–1891.
6 C. X. Wang, L. Xu, X. W. Xu, H. Cheng, H. C. Sun, Q. Lin and C. Zhang, *J. Colloid Interface Sci.*, 2014, **416**, 274–279.
7 C. Zhou, M. Long, Y. P. Qin, X. K. Sun and J. Zheng, *Angew. Chem., Int. Ed.*, 2011, **50**, 3168–3172.
8 L. B. Zhang and E. K. Wang, *Nano Today*, 2014, **9**, 132–157.
9 C.-L. Liu, H.-T. Wu, Y.-H. Hsiao, C.-W. Lai, C.-W. Shih, Y.-K. Peng, K.-C. Tang, H.-W. Chang, Y.-C. Chien, J.-K. Hsiao, J.-T. Cheng and P.-T. Chou, *Angew. Chem., Int. Ed.*, 2011, **50**, 7056–7060.
10 H.-H. Wang, C.-A. J. Lin, C.-H. Lee, Y.-C. Lin, Y.-M. Tseng, C.-L. Hsieh, C.-H. Chen, C.-H. Tsai, C.-T. Hsieh, J.-L. Shen, W.-H. Chan, W. H. Chang and H.-I. Yeh, *ACS Nano*, 2011, **5**, 4337–4344.
11 C. X. Wang, Y. Wang, L. Xu, X. D. Shi, X. W. Li, X. Xu, H. C. Sun, B. Yang and Q. Lin, *Small*, 2013, **9**, 413–420.
12 J. Bomm, C. Günter and J. Stumpe, *J. Phys. Chem. C*, 2012, **116**, 81–85.
13 L. Shang, F. Stockmar, N. Azadfar and G. U. Nienhaus, *Angew. Chem., Int. Ed.*, 2013, **52**, 11154–11157.
14 C. X. Wang, Z. Z. Xu, H. Cheng, H. H. Lin, M. G. Humphrey and C. Zhang, *Carbon*, 2015, **82**, 87–95.
15 G. Kucsko, P. C. Maurer, N. Y. Yao, M. Kubo, H. J. Noh, P. K. Lo, H. Park and M. D. Lukin, *Nature*, 2013, **500**, 54–59.
16 M. Mahmoudi, A. M. Abdelmonem, S. Behzadi, J. H. Clement, S. Dutz, M. R. Ejtehadi, R. Hartmann, K. Kantner, U. Linne, P. Maffre, S. Metzler, M. K. Moghadam, C. Pfeiffer, M. Rezaei, P. Ruiz-Lozano, V. Serpooshan, M. A. Shokrgozar, G. U. Nienhaus and W. J. Parak, *ACS Nano*, 2013, **7**, 6555–6562.

17 K. Ookabe, N. Inada, C. Gota, Y. Harada, T. Funatsu and S. Uchiyama, *Nat. Commun.*, 2012, **3**, 705–714.

18 A. E. Albers, E. M. Chan, P. M. McBride, C. M. Ajo-Franklin, B. E. Cohen and B. A. Helms, *J. Am. Chem. Soc.*, 2012, **134**, 9565–9568.

19 S. N. Qu, H. Chen, X. M. Zheng, J. S. Cao and X. Y. Liu, *Nanoscale*, 2013, **5**, 5514–5518.

20 V. A. Vlaskin, N. Janssen, J. van Rijssel, R. Beaulac and D. R. Gamelin, *Nano Lett.*, 2010, **10**, 3670–3674.

21 E. J. McLaurin, L. R. Bradshaw and D. R. Gamelin, *Chem. Mater.*, 2013, **25**, 1283–1292.

22 A. R. Bayles, H. S. Chahal, D. S. Chahal, C. P. Goldbeck, B. E. Cohen and B. A. Helms, *Nano Lett.*, 2010, **10**, 4086–4092.

23 S. P. Wang, S. Westcott and W. Chen, *J. Phys. Chem. B*, 2002, **106**, 11203–11209.

24 F. Ye, C. F. Wu, Y. H. Jin, Y.-H. Chan, X. J. Zhang and D. T. Chiu, *J. Am. Chem. Soc.*, 2011, **133**, 8146–8149.

25 F. Vetrone, R. Naccache, A. Zamarrón, A. J. Fuente, F. Sanz-Rodríguez, L. M. Maestro, E. M. Rodriguez, D. Jaque, J. G. Solé and J. A. Capobianco, *ACS Nano*, 2010, **4**, 3254–3258.

26 Y. X. Fang, S. J. Guo, D. Li, C. Z. Zhu, W. Ren, S. J. Dong and E. K. Wang, *ACS Nano*, 2011, **6**, 400–409.

27 S. J. Zhu, Q. N. Meng, L. Wang, J. H. Zhang, Y. B. Song, H. Jin, K. Zhang, H. C. Sun, H. Y. Wang and B. Yang, *Angew. Chem., Int. Ed.*, 2013, **52**, 3953–3957.

28 L. Shang, S. J. Dong and G. U. Nienhaus, *Nano Today*, 2011, **6**, 401–418.

29 A. W. Zhu, Q. Qu, X. L. Shao, B. Kong and Y. Tian, *Angew. Chem., Int. Ed.*, 2012, **124**, 7297–7301.

30 M. H. Lan, J. F Zhang, Y.-S. Chui, P. F. Wang, X. F. Chen, C.-S. Lee, H.-L. Kwong and W. J. Zhang, *ACS Appl. Mater. Interfaces*, 2014, **6**, 21270–21278.

31 E. G. Ju, Z. Liu, Y. D. Du, Y. Tao, J. S. Ren and X. G. Qu, *ACS Nano*, 2014, **8**, 6014–6023.

32 T. T. Chen, Y. H. Hu, Y. Cen, X. Chu and Y. Lu, *J. Am. Chem. Soc.*, 2013, **135**, 11595–11602.

33 C. X. Wang, L. Xu, Y. Wang, D. Zhang, X. D. Shi, F. X. Dong, K. Yu, Q. Lin and B. Yang, *Chem.–Asian J.*, 2012, **7**, 1652–1656.

34 W. Kwon, G. Lee, S. Do, T. Joo and S.-W. Rhee, *Small*, 2014, **10**, 506–513.

35 X. C. Jiang, T. Herricks and Y. N. Xia, *Adv. Mater.*, 2003, **15**, 1205–1209.

36 R. Tedja, A. H. Soeriyadi, M. R. Whittaker, M. Lim, C. Marquis, C. Boyer, T. P. Davis and R. Amal, *Polym. Chem.*, 2012, **3**, 2743–2751.

37 Y. Qin, L. Sun, X. Li, Q. Q. Cao, H. Wang, X. F. Tang and L. Ye, *J. Mater. Chem.*, 2011, **21**, 18003–18010.

38 A. Pandikumar, S. Murugesan and R. Ramara, *ACS Appl. Mater. Interfaces*, 2010, **7**, 1912–1917.

39 H. Cheng, C. X. Wang, Z. Z. Xu, H. H. Lin and C. Zhang, *RSC Adv.*, 2015, **5**, 20–26.

40 N. Nishida, E. S. Shibu, H. Yao, T. Oonishi, K. Kimura and T. Pradeep, *Adv. Mater.*, 2008, **20**, 4719–4723.

41 R. J. Zhou, M. M. Shi, X. Q. Chen, M. Wang and H. Z. Chen, *Chem.–Eur. J.*, 2009, **15**, 4944–4951.

42 C. X. Wang, Y. Wang, L. Xu, D. Zhang, M. X. Liu, X. W. Li, H. C. Sun, Q. Lin and B. Yang, *Small*, 2012, **8**, 3137–3142.

43 H. W. Gu, Z. M. Yang, J. H. Gao, C. K. Chang and B. Xu, *J. Am. Chem. Soc.*, 2005, **127**, 34–35.

44 C. X. Wang, D. Zhang, L. Xu, Y. N. Jiang, F. X. Dong, B. Yang, K. Yu and Q. Lin, *Angew. Chem., Int. Ed.*, 2011, **50**, 7587–7591.

45 S. Yang and H. R. Liu, *J. Mater. Chem.*, 2006, **16**, 4480–4487.

46 Y. Y. Wang, Y. Lei, J. Li, L. Gu, H. Y. Yuan and D. Xiao, *ACS Appl. Mater. Interfaces*, 2014, **6**, 6739–6747.

47 R. Lv, P. P. Yang, F. He, S. Gai, C. X. Li, Y. Dai, G. L. Yang and J. Lin, *ACS Nano*, 2015, **9**, 1630–1647.

48 Y. Chen, Y. Wang, C. X. Wang, W. Y. Li, H. P. Zhou, H. P. Jiao, Q. Lin and C. Yu, *J. Colloid Interface Sci.*, 2013, **396**, 63–68.

49 X. Y. Zhai, P. Zhang, C. J. Liu, T. Bai, W. C. Li, L. M. Dai and W. G. Liu, *Chem. Commun.*, 2012, **48**, 7955–7957.

50 Y. He, Y. L. Zhong, F. Peng, X. P. Wei, Y. Y. Su, Y. M. Lu, S. Su, W. Gu, L. S. Liao and S.-T. Lee, *J. Am. Chem. Soc.*, 2011, **133**, 14192–14195.

51 J. M. Yang, H. Yang and L. Lin, *ACS Nano*, 2011, **5**, 5067–5071.

52 S. Hedstrom, P. Henriksson, E. Wang, M. R. Andersson and P. Persson, *J. Phys. Chem. C*, 2015, **119**, 6453–6463.

53 H. Wang, J. Yi, S. Mukherjee, P. Banerjee and S. Zhou, *Nanoscale*, 2014, **6**, 13001–13011.

54 C. X. Li, D. M. Yang, P. Ma, Y. Y. Chen, Y. Wu, Z. Y. Hou, Y. L. Dai, J. H. Zhao, C. P. Sui and J. Lin, *Small*, 2013, **9**, 4150–4159.